https://doi.org/10.5194/egusphere-2023-1025
Preprint. Discussion started: 28 June 2023

Is transport of microplastics different from that of mineral dust? Results from idealized wind tunnel studies

Eike Maximilian Esders[1], Sebastian Sittl[2], Inka Krammel[2], Wolfgang Babel[1,3], Georg Papastavrou[2], and Christoph Karl Thomas[1,3]

[1]Micrometeorology Group, University of Bayreuth, Universitätsstraße 30, Bayreuth, Germany
[2]Department of Physical Chemistry II, Universtiy of Bayreuth, Universitätsstraße 30, Bayreuth, Germany
[3]Bayreuth Center of Ecology and Environmental Research, Dr.Hans-Frisch-Str.1-3, Bayreuth, Germany

Correspondence: Eike Esders (Eike.Esders@uni-bayreuth.de)

Abstract. Atmospheric transport disperses microplastic particulate matter to virtually every environment on the planet. Despite the well-known long-range transport, only few studies have examined the fundamental transport mechanisms for microplastics and contrasted it with the existing body of knowledge accumulated for mineral dust over the past decades. Our study addresses this research gap and presents results from wind tunnel experiments, which examine the detachment behavior of microplastics ranging from 38 to 125 μm in diameter from idealized substrates. We here define 'detachment' as microspheres detaching from a substrate and leaving the field of observation, which includes several transport modes including creeping, rolling, directly lifting off. The detachment behavior of polyethylene microspheres (PE69) and borosilicate microspheres (GL69) of nominally the same physical diameter (63-75 μm) are contrasted across hydrophilic to hydrophobic substrates. We further examine the effect of microsphere-microsphere collisions on the detachment behavior of both polyethylene and borosilicate microspheres. Differentiating between collision independent microspheres and collisions dependent microspheres revealed that collisions impact detachment from enhancing to mitigating. Further, results indicate that GL69, as a hydrophilic particle, is highly dependent on substrate hydrophobicity and PE69 is less affected by it. A more detailed comparison between GL69 and PE69 regarding surface and substrate hydrophobicity is masked by the influence of capillary forces. Moreover, the smallest polyethylene microspheres behave similar to mineral microspheres. Results demonstrate that PE69 and GL69 as proxy for plastic and mineral dust, respectively, detach at u_* between 0.1 to 0.3 ms^{-1} fitting to the prediction of the simple wind erosion model by Shao and Lu (2000). In the observed range of rH, capillary forces can increase the median detachment by about 0.2 ms^{-1} for PE69 and GL69. Polyethylene microspheres, smaller than 70 μm in diameter, behave like borosilicate microspheres of the same size. For bigger microspheres, the lesser density of polyethylene drives their higher erodibility. We conclude that it is no surprise, that like mineral dust, plastic dust is found all around the globe, transported via the atmosphere.

1 Introduction

Humans use plastics in virtually all their activities with the consequence of bringing around 4900 Mt of plastic waste into the environment from 1950 to 2015 (Geyer et al., 2017). Plastics are intentionally non-biodegradable and can persist in the environment for several centuries (Barnes et al., 2009). Exposed to the environment, plastic negatively affects individual organisms

https://doi.org/10.5194/egusphere-2023-1025
Preprint. Discussion started: 28 June 2023

(Alexiadou et al., 2019; Donnelly-Greenan et al., 2019) and ecosystems (Wang et al., 2022; Zhang et al., 2022; Windsor et al., 2019).

The present work focuses on microplastic, defined as plastic particles smaller than 5 mm in all dimensions. Based on their origin, microplastics are further subdivided into either primary microplastics, which are produced with sizes $\leq$ 5 mm, or secondary microplastics formed by degradation of larger plastic particles (Du et al., 2021; Meides et al., 2021; Weinstein et al., 2016).

Today, microplastics are found in animals (Thrift et al., 2022; Ugwu et al., 2021; Carlin et al., 2020), terrestrial systems (Chia et al., 2021; Xu et al., 2020), the atmosphere (Allen et al., 2021; Zhang, 2020) and in aquatic systems (Thushari and Senevirathna, 2020). Further, recent evidence shows microplastics move between aquatic, atmospheric and terrestrial systems (Rolf et al., 2022; Shiu et al., 2022; Boos et al., 2021; Lehmann et al., 2021; Rehm et al., 2021; Brahney et al., 2020; Kernchen et al., 2022; Evangeliou et al., 2020; Bank and Hansson, 2019; Horton and Dixon, 2018).

Compared to aquatic systems, microplastics transport and concentrations in terrestrial and atmospheric ecosystems have gained much less attention (Li et al., 2020). Strikingly, it is likely that arable soils alone contain more microplastics than the oceans (Rillig, 2012; de Souza Machado et al., 2018; Nizzetto et al., 2016). Further, arable soils are susceptible to wind erosion and thus potentially source areas for the atmospheric transport of microplastics (Tian et al., 2022; Yang et al., 2022; Rezaei et al., 2019). Regarding atmospheric transport of microplastics, most research has focused on atmospheric deposition (Zhang, 2020). Deposition was measured in cities (Shruti et al., 2022; Klein and Fischer, 2019; Dris et al., 2015) with typical deposition rates ranging between ≤ 5 and ≥ 1000 microplastics$\cdot m^{-2} d^{-1}$. Further, microplastics were found in remote environments such as the arctic, nature reserves, glaciers and the deep sea (Bergmann et al., 2019; Allen et al., 2019; Brahney et al., 2020; Stefánsson et al., 2021; Katija et al., 2017). Their distance to urban areas suggests that microplastics are transported via the atmosphere rather than via aquatic systems. So far, little is known about microplastic transport and dynamics in the atmosphere (Allen et al., 2022).

The atmospheric transport of microplastics starts with the detachment from a substrate. This process has only recently been studied. Tian et al. (2022) and Yang et al. (2022) presented studies conducted on arable land in northern China, which used novel flat open traps to collect in-situ wind-blown sand (saltation) and dust (suspension) during wind erosion events. Bullard et al. (2021) presented a series of wind tunnel experiments with prepared mixtures of soil, sand, and microplastics. Rezaei et al. (2019) used a movable wind tunnel to conduct controlled erosion experiments on arable and natural environments. The mentioned studies yielded enrichment ratios of microplastics and relate the concentration of microplastics in the original substrate to that in the transported soil. All findings showed that microplastics are preferentially transported by wind in comparison to the mineral soil. Typical enrichment ratios were found to be as high as 16.6 for fragments, and up to 726 for fibers. The relative lower density of any microplastic and the elongated form of microplastic fibers are hypothesized to drive the preferential transport resulting in the high enrichment ratios.

The presented explorative studies are the first step in uncovering the mechanisms driving the atmospheric transport of microplastics, which requires investigating the fundamental mechanisms of their movement in the environment. As a start, the present work investigates the detachment of a monolayer of factory-fresh plastic microspheres and borosilicate microspheres

https://doi.org/10.5194/egusphere-2023-1025
Preprint. Discussion started: 28 June 2023

from substrates with hydrophilic to hydrophobic surfaces in a series of wind tunnel experiments. By studying the detachment behavior of the microspheres, the influence of material properties and relative humidity (rH) on the erodibility of both microsphere types will be elucidated.

A microsphere on a substrate is influenced by gravity, adhesion, aerodynamic drag and aerodynamic lift. Gravity and adhesion are the retarding forces. For microspheres smaller than 50 μm, the force of adhesion is at least 100 times larger than the gravitational force (Shao and Lu, 2000), which becomes relevant for microspheres larger than 100 μm in size. Further, adhesion has a non-linear relation to relative humidity. At some critical relative humidity (rH_c), capillary forces occur, due to water accumulating between microsphere and substrate. When capillary forces are present, adhesion is increased, but when capillary forces are not present, adhesion is constant and independent of rH (Rabinovich et al., 2002; Kim et al., 2016; Ibrahim et al., 2004; Corn and Stein, 1965). Thus, rH must be known to interpret the detachment of microspheres from a substrate. At best, laboratory studies control rH and directly compute rH_c. In the presented work, rH was monitored during the experiments, but controlling the moisture content of the air was outside the scope and technical possibilities for airflows of several thousand m^3h^{-1}. Nonetheless, natural, weather-driven variations of rH during the experimental phase allowed us to evaluate a wide range of relative humidities since the air entering the wind tunnel communicated with outside conditions.

Aerodynamic drag and aerodynamic lift are the detaching forces. These two aerodynamic forces are related to the shear forces close to the surface, and hence are functions of the density-normalized momentum flux, termed the friction velocity (u_*). When the detaching forces overcome the retarding forces, a microsphere can be detached from the substrate it rests upon. At this critical friction velocity for a single microsphere ($u^c_{*,i}$), the lift forces are sufficient to detach it. When a single microsphere detaches from a substrate, it can roll, slide or lift off directly (Kassab et al., 2013). The critical friction velocity increases from rolling to sliding to directly lifting-off (Ibrahim et al., 2004; Soltani and Ahmadi, 1994). Consequently, most detached microspheres either roll or slide on the substrate and collisions between moving microspheres and stationary microspheres are likely. Thus, when multiple microspheres are observed, we also need to consider another detaching force in our investigations resulting from the microsphere-microsphere collisions, hereafter simply referred to as collisions. Ibrahim et al. (2004) showed that collisions effectively detach microspheres and that moving microspheres can transfer more kinetic energy onto a stationary microsphere during collision compared to the acting aerodynamic forces. Thus, collisions lead to detaching microspheres for $u_* < u^c_{*,i}$. Similarly, a moving microsphere can be stopped by a stationary microsphere, when the collision impulse is insufficient to overcome the binding forces.

The main motivation of the work presented here is driven by the questions i) to what extent influence collisions, surface properties, and relative humidity the critical friction velocity u^c_* of PE and borosilicate microspheres? And ii) if the findings support the preferential transport of microplastics found in former studies?

https://doi.org/10.5194/egusphere-2023-1025
Preprint. Discussion started: 28 June 2023

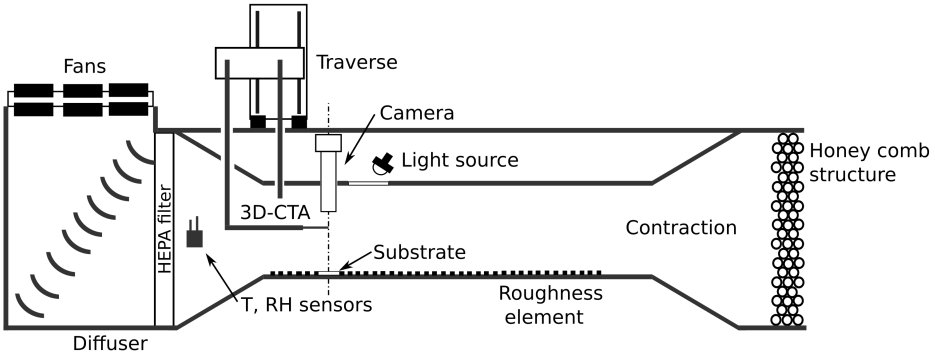

Figure 1. Schematic of the wind tunnel to observe microsphere detachment.

2 Methods

2.1 Wind tunnel and camera equipment

The non-circulating wind tunnel used in this study was 730 cm long, 60 cm wide and 120 cm high (see Fig. 1). Air is sucked sequentially through a contraction section (cross-section dimensions of 54 cm x 27 cm; contraction ratio 5:1; honeycomb structure ensuring laminar flow conditions), a test section (substrate mount, camera, constant temperature anemometer and light source), and a deflector section (HEPA filter; temperature and relative humidity sensors). The outlet held twelve fans of diameter 26.5 cm (RAB O TURBO 250, DALAP GmbH, Germany), whose rotation speed was controlled using a stepless transformer (LSS 720-K, Thalheimer Transformatoren GmbH, Germany). The rotation speed of the fans controlled the airflow speed in the wind tunnel. The air was filtered by a HEPA filter (EU2, 10 μm pore size, Erwin Telle GmbH, Germany), before it was released to the laboratory.

A roughness element, installed for turbulence production, covered most of the test section's floor (170 cm). The roughness element was equipped with a substrate mount such that its surface containing the microspheres was at the same vertical height as the top of the roughness element. The background of the substrate mount was painted with a high emissivity resistant black paint for high contrast between microspheres and image background (HERP-LT-MWIR-BK-11, LabIR, Czech Republic). Above the substrate mount a constant temperature anemometer (CTA) (three-dimensional hot wire probe, Model 55P095, Dantec Dynamics, controller, Model 54T42, Dantec Dynamics) measured the turbulent flow statistics. The deflector section redirected the air to the outlet of the wind tunnel. In the deflector section, air temperature and rH were measured using a slow-response thermohygrometer (Model HC2A, rotronic). In addition, the CTA was equipped with a fast-response air thermometer (Model 90P10, Dantec Dynamics) located in proximity to the test substrates.

The free-stream velocity could be varied from zero up to 11 ms^{-1}. The free stream turbulence intensity (I), defined as:

$$I = \sigma_u / \bar{U},$$

where σ_u is the standard deviation of u and $\bar{U}$ is the horizontal mean velocity, was less than 1 % over the entire velocity range.

https://doi.org/10.5194/egusphere-2023-1025
Preprint. Discussion started: 28 June 2023

Microsphere detachment was captured with a camera (Model Sony Alpha 7 RII, Sony) equipped with a long-distance microscopy lens (K2 DistaMax, with a CF1 lens, Infinity, USA). The long-distance microscope lens captured images with a magnification ratio of up to 1:1 at an object distance of 35 cm. The photo equipment did not disturb the flow field due to its large distance to the substrate. The field of observation was 861.6 mm^2. Images were taken every 10 seconds and were directly transferred and stored on a PC. Experiments were conducted at an air temperature of 23 $\pm$ 2 °C and a rH from 20 % to 60 %.

2.2 Turbulence characteristics

The vertical velocity profiles showed a typical boundary-layer velocity profile for a channel flow (see Fig. A5). The friction velocity and roughness length were calculated for z $\leq$ 21 mm, where the velocity profile agrees well with the logarithmic law of the wall. The roughness length (z_0) was calculated by extrapolating the logarithmic wind profile:

$$\bar{U}(z) = \frac{u_*}{\kappa} ln\left(\frac{z}{z_0}\right)$$

to the height z where $\bar{U}$ = 0, giving z_0 = 0.5 mm.

The friction velocity (u_*) was computed against the free-stream velocity (U_∞). The velocity was regressed by a least-squares linear algorithm to

$$u_* = 0.06 \cdot U_\infty,$$

where the uncertainty in u_* is 0.02 ms^{-1} for the 99.7 % percentile.

2.3 Determining detachment from measurements

Detachment of microspheres was measured as the decreasing number of microspheres in the field of observation. The algorithm used to quantitatively determine the number of microspheres in each individual image is described in Esders et al. (2022). In a single experiment, up to approximately 1500 microspheres were placed on a substrate as described above, positioned in the wind tunnel on the substrate mount, and subsequently exposed to airflows with increasing friction velocities. The friction velocity (u_*) increased step-wise from 0 to 0.65 ms^{-1} while it was held constant for 360 s at each step. The increments in u_* were selected such that at every step more than 10 % of the initial number of microspheres, but less than 30 % were detached to optimize the statistics on moving microspheres. A single experiment comprised about 200 images.

2.4 Microspheres and substrates

We used polyethylene and borosilicate microspheres to address our research questions. Three differently sized spherical fluorescent plastic microspheres made of polyethylene (density: 1025 kgm^{-3}; Cospheric LLC, United States) were used with the following diameters: 38-45 μm (hereafter referred to as PE42), 63-75 μm (hereafter referred to as PE69), and 106-125 μm (hereafter referred to as PE115). The borosilicate microspheres with diameters 63-75 μm were used (density: 2200 kgm^{-3}; Cospheric LLC, United States), hereafter referred to as GL69.

https://doi.org/10.5194/egusphere-2023-1025
Preprint. Discussion started: 28 June 2023

Substrate	Θ_S (°)	Cleaning procedure	Coating
a	<30	RCA	no coating
b	55 ± 5	Ibrahim et al. 2003	no coating
c	65 ± 1	RCA	3-aminopropyldimethylethoxysilane
d	120 ± 1	RCA	1H-1H-2H-2H perfluorodecyltrichlorosilane

Table 1. Overview of the four types of substrates used in the experiments. The static contact angles (Θ_S) of substrates with a water droplet indicate hydrophilicity or hydrophobicity. A small Θ_S indicates a hydrophilic, a high Θ_S indicates a hydrophobic substrate. Substrates were cleaned according to a protocol developed by the radio corporation of america (RCA) Kern (1990) or a cleaning procedure described in Ibrahim et al. (2003). Substrates c and d were coated with 3-aminopropyldimethylethoxysilane and 1H-1H-2H-2H perfluorodecyltrichlorosilane, respectively, after the cleaning procedure.

Comparing PE69 and GL69, is especially interesting, as they have the nominal same diameter. We chose them as the directly compared proxies for plastic and mineral dust. For PE69 and GL69, the root-mean-square roughness was determined, being 248.5 ± 32.2 nm and 27.7 ± 9.0 nm, respectively. See the appendix, for scanning electron microscopy images and atomic force microscopy images of both microsphere types.

The microspheres were detached from glass plates as substrate material (76×26 mm, Thermo Scientific; 76×26 mm, VWR). Substrates with hydrophobic to hydrophilic surfaces were prepared by cleaning and subsequent optional coating (see Tab. 1). The hydrophobicity of a substrate was characterized by its static contact angle with a water droplet (Θ_S) using the sessile drop method (Dataphysics, Contact Angle System OCA, Filderstadt, Germany). A substrate with a small Θ_S is hydrophilic and with a high Θ_S is hydrophobic. A detailed preparation procedure for each substrate is described in the supplemental information.

The microspheres were deposited via gravitational settling as a monolayer on the substrates. Substrates were prepared outside the wind tunnel. Deposition was made immediately before the start of an experiment to minimize the residence time of the microspheres, as residence time can suppress detachment (Ibrahim et al., 2004). A self-made template (see Fig. A1) for microspheres deposition, ensured that all microspheres were deposited in the field of observation (see Fig. 2). In over 30 runs, on average 1490 ± 950, 647 ± 490, 366 ± 165 and 1164 ± 514 microspheres were deposited in the field of observation for PE42, PE69, PE115 and GL69 respectively, resulting in a number density of microspheres from 0.2 to 1.7 microspheres per mm^2 on average.

A UV-light (LED SLS-6 UV Floor, eurolite, Germany) was used to excite fluorescent microspheres, while a daylight lamp (Lumilux Cool Daylight, L18W/865, Osram, Germany) was used to expose the borosilicate microspheres.

2.5 Characteristic microsphere statistical quantities

The results relate the detached fraction to the friction velocity of the turbulent airflow. This fraction is defined as,

$$N_*(u_*) = 1 - \frac{N(u_*)}{N(0)},$$

https://doi.org/10.5194/egusphere-2023-1025
Preprint. Discussion started: 28 June 2023

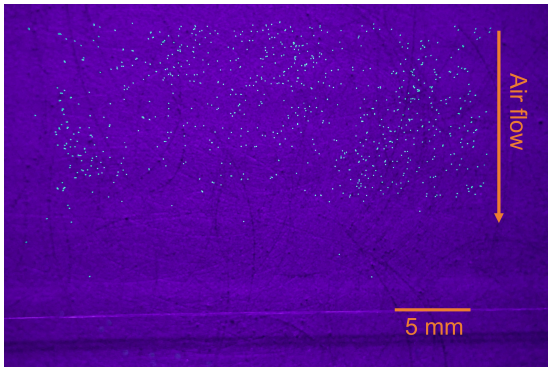

Figure 2. Typical substrate just before an experiment, here equipped with polyethylene microspheres with 63 μm to 75 μm in diameter. In respect to the image, air flows from top to bottom.

where $N(u_*)$ is the number of non-detached microspheres on the substrate, after it was exposed to a friction velocity u_* and $N(0)$ is the initial number of microspheres on the substrate. A logistic function of the following form was fit to the results of individual experiments,

$$N_*(u_*) = \frac{A}{1 + e^{-b \cdot (u_* - m)}}$$

where A is the function's maximum value, b is the logistic growth rate and m is $\frac{A}{2}$. The fit allowed to evaluate $N_*(u_*)$ at any u_* which allowed for comparison between individual runs. Further, the relative number of detached microspheres is defined as:

$$N_*(t) = 1 - \frac{N(t)}{N(0)},$$

where $N(t)$ is the number of non-detached microspheres on the substrate at time t and $N(0)$ is the initial number of microspheres on the substrate (t = 0). In addition, the threshold friction velocity ($u_{*,th}$) is defined as the value at which 50 % of all microspheres detach. We use this value to represent the overall detachment behavior.

Note that a population of microspheres detaches over a range of velocities rather than at a specific single velocity. An individual microsphere experiences an individual force of adhesion depending on its exact diameter and its surface roughness in relation to that of the substrate and hence has an individual critical friction velocity ($u^c_{*,i}$). Further, the stochastic nature of the turbulent airflow exerts a homogenous force onto the substrate when averaged over longer time scales, while on short time scales its substantial spatio-temporal variability is large.

2.6 Determining the effect of collisions on detachment

Collisions between microspheres were likely as initial number densities of deposited microspheres reached up to 1.7 microsphere $\cdot$ mm^{-2} and certainly impacted the detachment statistics reported below. Two cohorts of microspheres were defined to study the effect of collisions on detachment. The first cohort excluded the effect of collisions on detachment, while the second cohort included the effect of collisions on detachment specifically. For the first cohort, the most windward microspheres in

https://doi.org/10.5194/egusphere-2023-1025
Preprint. Discussion started: 28 June 2023

the field of observation in the first image were determined. For each subsequent image, the decrease in these particles was registered. The results of this analysis are referred to as cohort collisions independent microspheres (CIMs). The algorithm is described in detail in the appendix. Note that, the most windward microspheres cannot be impacted by downwind moving microspheres. Hence, CIMs show the distribution of retarding forces on the scale of an individual microsphere, hereafter referred to as the individual scale. For the second cohort, all microspheres in the field of observation were counted, but the remaining CIMs were subtracted. The results of this analysis are referred to as cohort collision dependent microspheres (CDMs). CDMs show how collisions influence the detachment of a population of microspheres, hereafter referred to as the population scale. In over 30 runs, on average 60 $\pm$ 14, 55 $\pm$ 17, 50 $\pm$ 14 and 68 $\pm$ 15 microspheres were recognized as CIMs for PE42, PE69, PE115 and GL69, respectively. The ratio of the $u_{*,th}$ for CIMs to the $u_{*,th}$ for CDMs, hereafter, is referred to as α.

2.7 Predicting critical friction velocities from a model

In addition to $u^c_{*,i}$, a critical friction velocity for multiple microsphere (u^c_*) can be determined, that marks the start of sustained detachment. Shao and Lu (2000) proposed a model, that predicts the start of detachment for a soil that is made up of uniform, spherical microspheres that are spread loosely over a dry and flat substrate. We assume that a glass plate as a substrate equipped with a monolayer of microspheres represents a simplified soil. Thus, we consider the Shao model a fitting predictor for the simplified soils used in this study. The model was used in the following form:

$$u^c_* = \sqrt{A_N(\sigma_\rho g d + \frac{\gamma}{\rho d})},$$

where A_N = 0.0123, σ_ρ is the ratio of the microsphere's density to the density of air, g is the gravitational acceleration, d is the diameter and γ is 3 * 10^{-4}kgs^{-2}. This model was used to predict u^c_* for the median diameters of the microspheres studied in this paper. Predicting u^c_* provides a theoretical reference for the experimental results.

Determining u^c_* from experimental results is not obvious. Ravi et al. (2004) or Mckenna Neuman (2003) determined u^c_* as the friction velocity, at which the transport rate of particles increases significantly in magnitude, say 100 particles per second compared to single particles per second. In the presented study, about 50 collisions independent microspheres were examined per experiment. Thus, choosing an identical friction velocity for our experiments was impossible. We therefore determined u^c_* as the friction velocity at which 25% of particles detached, $N_*(u_*) = 0.25$ ($u_{*,Q1}$). We chose this definition as a quantifiable portion of particles already detached at this point, but the majority of particles will detach at higher friction velocities. The chosen $u_{*,Q1}$ therefore marks the start of detachment.

3 Results and Discussion

We first explain the effects of collisions on the overall detachment behavior. Then, we compare the experimental results to the model predictions for critical friction velocities. Finally, the experimental results across the range of hydrophilic to hydrophobic substrates are presented and discussed.

https://doi.org/10.5194/egusphere-2023-1025
Preprint. Discussion started: 28 June 2023

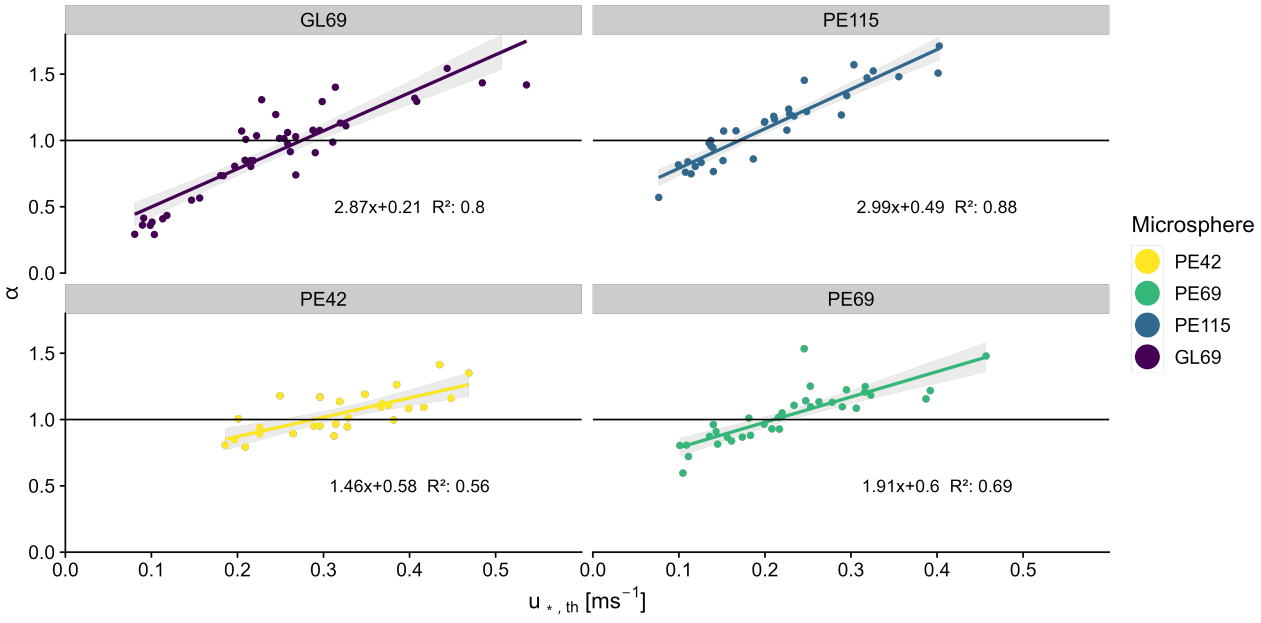

Figure 3. The ratio of the median detachment ($u_{*,th}$) for collision independent microspheres (CIMs) to collision dependent microspheres (α) as a function of $u_{*,th}$ for CIMs. Results are shown for all individual experiments with polyethylene microspheres with diameters: 38-45 μm (PE42), 63-75 μm (PE69), and 106-125 μm (PE115) and borosilicate microspheres with diameters 63-75 μm (GL69).

3.1 Influence of collisions on detachment

Figure 3 shows the ratio α of individual experiments as a function of the respective CIMs $u_{*,th}$. Here, α positively correlates with $u_{*,th}$ for all microspheres.

As mentioned above, in a collision, the stationary microsphere can be detached or the rolling microsphere can be stopped. Note that only CDMs see the effect of collisions. For GL69, at $u_{*,th}$ about 0.1 ms^{-1} α is about 0.5. A small $u_{*,th}$ indicates that microspheres detach and roll at low u_*, which results in a lower impulse than necessary for detaching stationary microspheres. Thus, the stationary microsphere stops the rolling microsphere. Hence, at low $u_{*,th}$ CIMs have smaller $u_{*,th}$ than CDMs. The opposite is true at high $u_{*,th}$. Here, microspheres detach at high u_* and the impulse is sufficient for detaching stationary microspheres. Thus, the rolling microsphere detaches a stationary microsphere at a friction velocity smaller than its critical friction velocity $u_* < u^c_{*,i}$. Hence, at high $u_{*,th}$ CIMs have higher $u_{*,th}$ than CDMs. To summarize, the ratio α indicates what kind of collisions occurred. If α is bigger than one, rolling microspheres detach stationary microspheres. If α is smaller than one rolling microspheres are stopped by stationary microspheres.

Understanding the impact of collisions on $u_{*,th}$ is important, when interpreting the impact of substrate hydrophobicity in Sect. 3.3.

https://doi.org/10.5194/egusphere-2023-1025
Preprint. Discussion started: 28 June 2023

3.2 Prediction and experimental results

The Shao model predicts a non-linear increase in u_*^c for $d < 100\mu\text{m} < d$ for PE microspheres and for $d < 70\mu\text{m} < d$ for borosilicate microspheres (see Fig. 4). The non-linear increase in u_*^c for larger microspheres cannot be observed due to the limit of the x-axis. The model further predicts that borosilicate microspheres detach at higher friction velocities than PE microspheres for roughly $d > 20\mu$m. The results presented here are all from experiments with substrate b. We found that $u_{*,Q1}$ values decrease with increasing diameter. The larger PE69 and PE115 show a similarly small $u_{*,Q1}$, while GL69 detach at higher $u_{*,Q1}$ compared to PE69. For PE69 and PE115, the detachment started at lower u_* than predicted. Differences in $u_{*,Q1}$ between CIMs and CDMs are small. Note that the results are slightly shifted on the x-axis for reasons of clarity. The dashed lines indicate the true position.

Considering the assumptions of the Shao model, it is conceivable that it overpredicts u_*^c compared to our observation. In the experiments, microspheres are placed in a monolayer, while the Shao model originates from the notion of multilayered microspheres. If microspheres are organized in multiple layers, microspheres rest on each other, with top ones resting in the troughs between the lower. When located in the trough, the top microspheres are not fully exposed to the airflow. Hence, only a part of the microsphere's cross-section normal to the airflow experiences drag. Thus, the drag onto the multilayered microspheres is smaller compared to microspheres in a monolayer, which experience drag on the complete cross-section normal to the airflow. Further, as a top microsphere sits in a trough, it has to be lifted out of it to be transported downstream. In a monolayer, a microsphere can simply start rolling. The process of lifting a microsphere requires more energy, than initiating a rolling motion on a flat surface. Moreover, in a multilayer, a top microsphere is in contact with multiple microspheres and hence experiences a sum of cohesive forces. In a monolayer, a microsphere experiences an adhesive force only by the substrate. If a microsphere in a multi- or monolayer experiences higher or lower adhesion or cohesion depends on the surface energy of the individual microsphere and substrate. Thus, it is not obvious, in which case higher u_*^c can be expected. The reduced drag and additional energy required for lifting a microsphere increase the u_*^c for an individual microsphere. Thus, it is reasonable that u_*^c are expected at higher u_* by the Shao model.

Further, PE69 and GL69 are no perfect spherical microspheres. Both microsphere types have surface roughness on the nanometer scale. Moreover, PE69 had significantly higher surface roughness than GL69. Surface roughness is not included in the model by Shao. To our knowledge, the impact of nanometer surface roughness on detachment of microspheres in these sizes has not been previously studied. Comparison with the Shao model shows that the observed u_*^c values are close to the expected values. Arguing nanometer surface roughness does not significantly alter u_*^c of PE69 and GL69, it does have some unexplained effect.

Still, predicted and experimentally determined critical friction velocities are well within the same order of magnitude. Thus, the experimental setup reproduces theoretically expected behavior and allows for further conclusions.

https://doi.org/10.5194/egusphere-2023-1025
Preprint. Discussion started: 28 June 2023

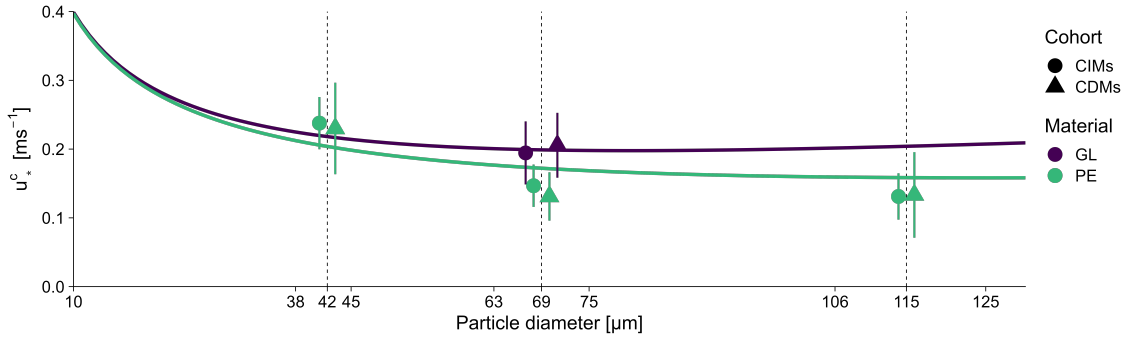

Figure 4. The critical friction velocity (u_*^c) as a function of microsphere diameter. The prediction of u_*^c from the model of Shao and Lu (2000) is represented by the solid lines. The results for collision independent microspheres (CIMs) and collision dependent microspheres (CDMs) are marked with triangles and dots, respectively. Note the non-linear relationship between u_*^c and the diameter. Box plots represent the $u_{*,Q1}$ of polyethylene microspheres: 38-45 μm (PE42), 63-75 μm (PE69), and 106-125 μm (PE115) and borosilicate microspheres 63-75 μm (GL69).

3.3 Substrate hydrophobicity and relative humidity

Figure 5 shows the detachment behavior of GL69 and PE69 in relation to Θ_S. Two dashed lines indicate the predicted u_*^c by the Shao model for PE69 and GL69 for general reference. The mean $u_{*,th}$ varies between 0.1 ms^{-1} and 0.3 ms^{-1} across all substrates. CIMs and CDMs of the individual microspheres have similar $u_{*,th}$ with a 0.05 ms^{-1} difference, except for GL69 on substrate d with a 0.15 ms^{-1} difference. Further, for PE69 (CIMs and CDMs), and for GL69 (CDMs) $u_{*,th}$ varies little with Θ_S. On the contrary, for GL69 (CIMs) $u_{*,th}$ decreases with Θ_S. For CDMs, borosilicate microspheres detach at higher $u_{*,th}$ compared to polyethylene microspheres. For CIMs, borosilicate microspheres detach at lower $u_{*,th}$ for $\Theta_S \geq 65°$ compared to polyethylene microspheres.

We expect, in general, that $u_{*,th}$ decreases with increasing hydrophobicity, as adhesion decreases and rH_c increases. Further, PE69, should detach at smaller $u_{*,th}$ compared to GL69, due to its lower density. However, the results show a more complex pattern, which requires considering microsphere hydrophobicity, capillary forces, surface roughness, and collisions.

For GL69, detaching collisions on substrate a and stopping collisions on substrate d hide the influence of Θ_S for CDMs. PE69, on the other hand, does not exhibit dependence on Θ_S for neither CIMS nor CDMs. Further, the results show that for GL69 on substrate a and for PE69 on substrate c, $u_{*,th}$ increases with rH (see. Fig. 6 and Fig. 7). No other variable changed. Therefore, we deduce that capillary forces increase $u_{*,th}$ at around 30% rH for PE69 and GL69. For substrate d, we expected the lowest $u_{*,th}$ for GL69 and PE69. However, only GL69 has the lowest $u_{*,th}$ for CIMs, whereas PE69 has high $u_{*,th}$ regardless of the cohort (see Fig. 8). For PE69, the high rH of 55% suggests that capillary forces increased $u_{*,th}$.

Results demonstrate that PE69 and GL69 as proxy for plastic and mineral dust, respectively, detach at u_* between 0.1 to 0.3 ms^{-1}. In the observed range of rH, capillary forces can increase $u_{,th}$ by about 0.2 ms^{-1} for PE69 and GL69. Considering only the diameter and density, PE69 should detach at lower $u_{*,th}$ than GL69 according to the explored model. Further, GL69,

https://doi.org/10.5194/egusphere-2023-1025
Preprint. Discussion started: 28 June 2023

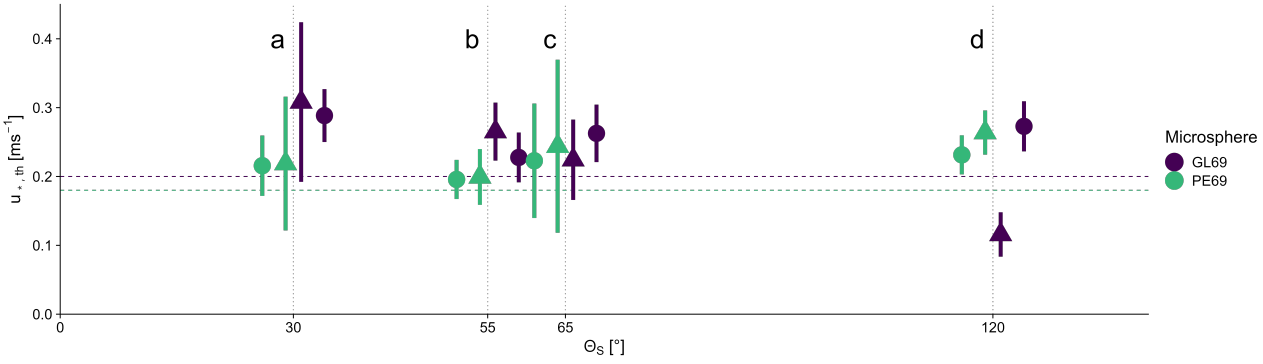

Figure 5. The threshold friction velocity ($u_{*,th}$) as a function of the substrate's hydrophobicity. Detachment is contrasted for polyethylene microspheres and borosilicate microspheres on a range of hydrophilic to hydrophobic substrates. The hydrophobicity is defined as the static contact angle between the substrate and a water droplet (Θ_S) using the sessile drop method. Hydrophobicity increases from small to high angles. Indices a to d indicate the individual substrates according to Tab. 1.

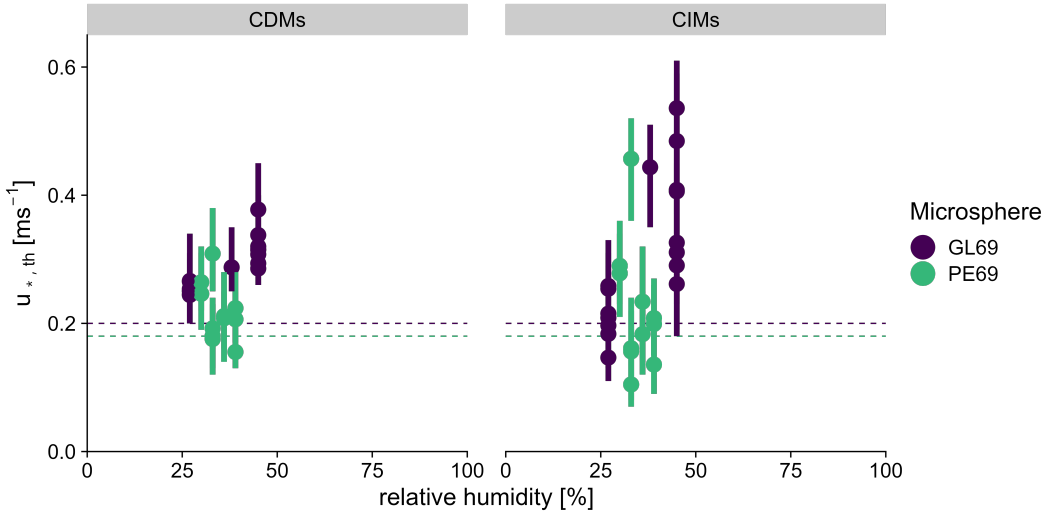

Figure 6. The threshold friction velocity ($u_{*,th}$) as a function of relative humidity (rH). Detachment is contrasted for polyethylene microspheres and borosilicate microspheres on substrate a.

https://doi.org/10.5194/egusphere-2023-1025
Preprint. Discussion started: 28 June 2023

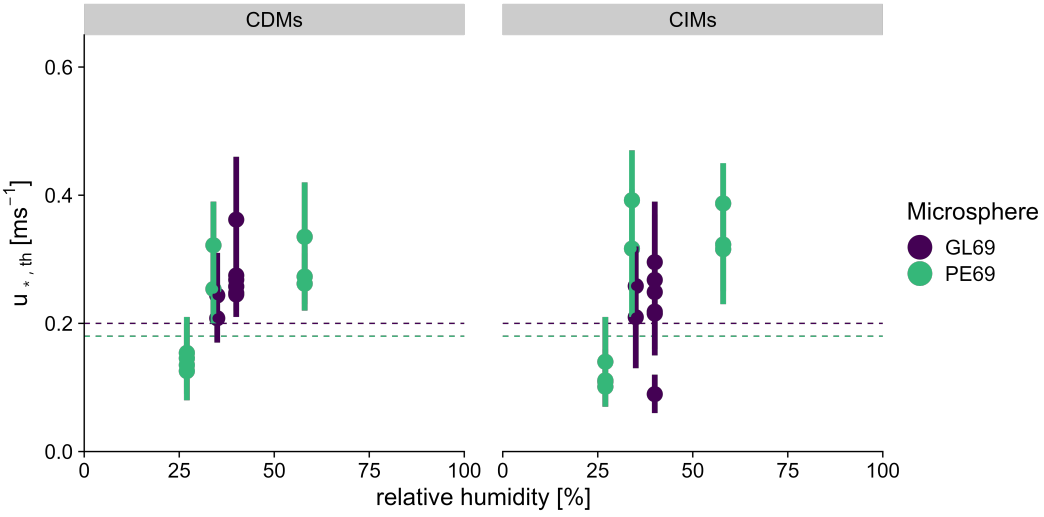

Figure 7. The threshold friction velocity ($u_{*,th}$) as a function of relative humidity (rH). Detachment is contrasted for polyethylene microspheres and borosilicate microspheres on substrate c.

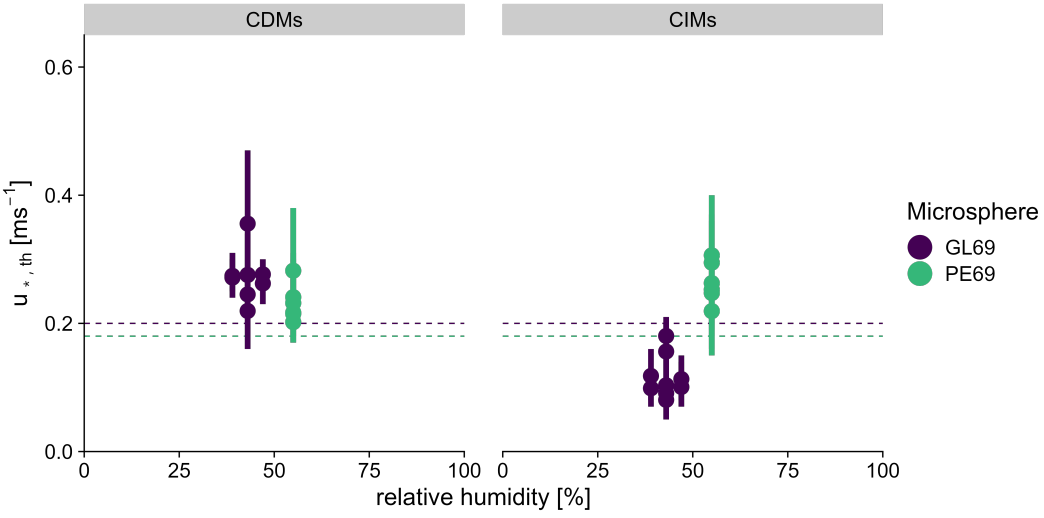

Figure 8. The threshold friction velocity ($u_{*,th}$) as a function of relative humidity (rH). Detachment is contrasted for polyethylene microspheres and borosilicate microspheres on substrate d.

https://doi.org/10.5194/egusphere-2023-1025
Preprint. Discussion started: 28 June 2023

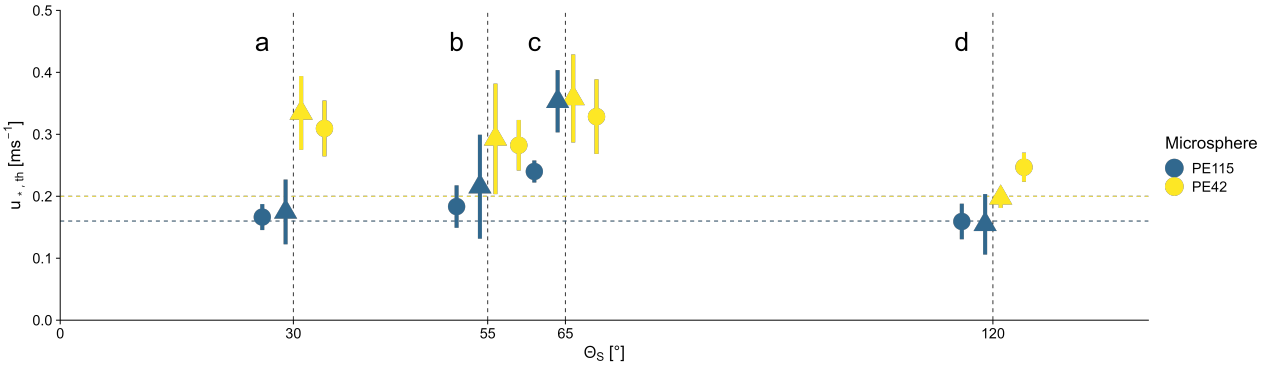

Figure 9. The threshold friction velocity ($u_{*,th}$) as a function of the substrate's hydrophobicity. Detachment is contrasted for polyethylene microspheres with diameters: 38-45 and 106-125 μm. Microspheres are detached from hydrophilic to hydrophobic substrates. The hydrophobicity is defined as the static contact angle between the substrate and a water droplet (Θ_S) using the sessile drop method. Hydrophobicity increases from small to high angles. Indices a to d indicate the individual substrates according to table 1.

as a hydrophilic particle, is dependent on Θ_S on the individual scale, whereas PE69 is less affected by Θ_S. A more detailed comparison between GL69 and PE69 regarding surface and substrate hydrophobicity is masked by the influence of capillary forces. If measured at the same rH, we would expect PE69 to detach at smaller $u_{,th}$, due to its lower density and hydrophobic surface.

3.4 Impact of microsphere diameter on retarding forces

The diameter of a microsphere determines which force dominates as retarding force. For PE42, we expect that it is more dependent on Θ_S than PE115, as adhesion dominates. On the contrary, for PE115 gravity dominates, and thus we expect little variation with Θ_S. The relation of $u_{*,th}$ to Θ_S for PE42 and PE115 is shown in Fig.9. At the observed range of Θ_S, PE42 detaches at higher $u_{*,th}$ and $u_{*,th}$ decreases with Θ_S for both CIMs and CDMs. The bigger PE115 detach at lower $u_{*,th}$ and $u_{*,th}$ varies little with Θ_S. Both PE42 and PE114 show a high $u_{*,th}$ on substrate c. Differences between CIMs and CDMs are small, except for PE115 on substrate c.

The high $u_{*,th}$ values on substrate c, found for both microsphere types, are unexpected. For experiments on substrate c, we found no variable, that would explain the high $u_{*,th}$ by theory or by correlation. Except for substrate c, the relation of $u_{*,th}$ and Θ_S for PE42 and PE115 fit our expectations. The bigger PE115 are less influenced by Θ_S and $u_{*,th}$ are close to the prediction by the Shao model. The smaller PE42 are dependent on Θ_S and $u_{*,th}$ decreases with increasing Θ_S. Here, no indication for the occurrence of capillary forces increasing $u_{*,th}$ is present (see Fig. A4).

In addition to the results of Sect. 3.2, showing that smaller PE42 microspheres detach at similar velocities to mineral microspheres independent of their density, here the results suggest that the adhesion dominated PE42 microspheres are sensitive to the substrate's hydrophobicity.

https://doi.org/10.5194/egusphere-2023-1025
Preprint. Discussion started: 28 June 2023

4 Conclusions

Future experiments should cover a wider range of relative humidities and the same relative humidities for all used microspheres. Further, microspheres should have similar surface roughness or an intentional range of surface roughness, to examine the effect of surface roughness on the detachment behavior. These improvements would allow for a more precise comparison of the detachment behavior of plastic and mineral particles.

We demonstrate that the detachment behavior on the individual scale and population scale can differ significantly. Collisions can promote or mitigate detachment. This, stresses that one should be aware, that collisions significantly affect the results when doing similar experiments.

The results are in good agreement with the prediction of the simple wind erosion model by Shao and Lu (2000). The good agreement confirms that a glass plate equipped with a monolayer of microspheres represents a simplified soil, and thus our experimental results should be transferable to the environment. Hence, plastic dust particles, smaller than 70 μm in size, behave similar to mineral dust particles of that size. For bigger particles, the lesser density of plastic drives their higher erodibility. We conclude that it is no surprise, that like mineral dust, plastic dust is found all around the globe, transported via the atmosphere.

Code and data availability. The image data of a single experiment and the code to analyze it are available at https://doi.org/10.5281/zenodo.7936729

Appendix A

A1 Deposition template

A self-made template for microspheres deposition, ensured that all microspheres were deposited in the field of observation (see Fig. A1). When a substrate is placed in the template, the template covers the substrate, while remaining an uncovered area for particle deposition (see Fig. A2).

A2 Substrate preparation

Glass plates (dimensions of 76×26 mm, Thermo Scientific;76×26 mm, VWR) were used as substrate material. Substrates were prepared in different fashions, thus a range from hydrophobic to hydrophilic substrates were available. The hydrophobicity of a substrate is characterized by its static contact angle with a water droplet (Θ_S). Contact angle measurements were conducted using the sessile drop method (Dataphysics, Contact Angle System OCA, Filderstadt, Germany).

Before functionalization, all substrates were cleaned using a cleaning procedure popularized by the radio corporation of america (Kern, 1990). First, the glass slide is sonicated in a 2 vol-% solution of Hellmanex III (Helma, Mühlheim, Germany) in Milli-Q water for ten minutes at 40°C and then rinsed with Milli-Q water (Merck IQ 7000, Darmstadt, Germany). It is then sonicated in a solution of Isopropanol (≥99.7%, CAS: 67-63-0, Bernd Kraft, Duisburg, Germany) and Milli-Q water in a volumetric ratio of 1:3 for ten minutes at 40°C and is again rinsed extensively with Milli-Q water. Lastly, the substrate is

https://doi.org/10.5194/egusphere-2023-1025
Preprint. Discussion started: 28 June 2023

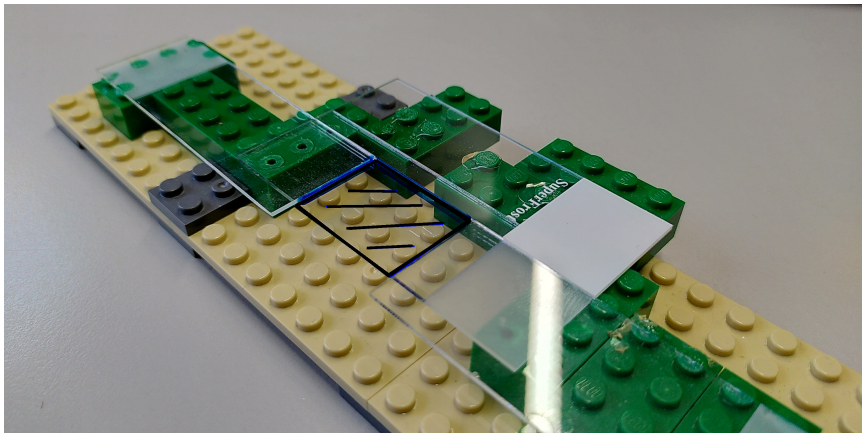

Figure A1. Close up on the self-made template for precise particle deposition. A substrate is placed in the template. The marked area represents the uncovered area for particle deposition.

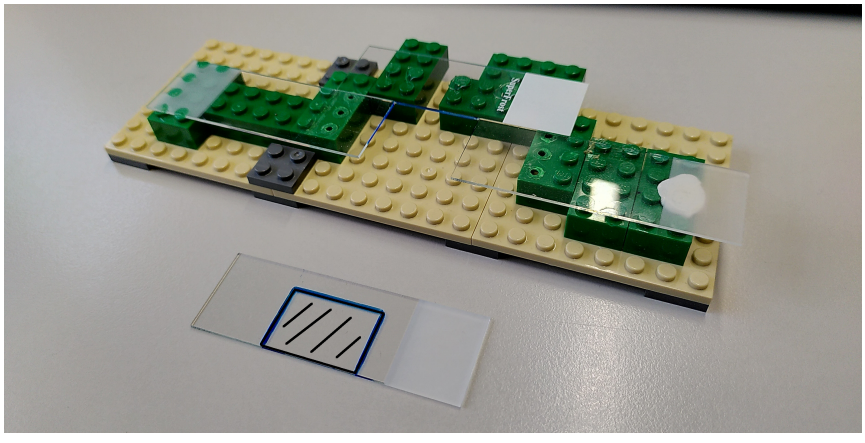

Figure A2. Self-made template and substrate. The marked area represents the uncovered area for particle deposition.

placed in a mixture of Milli-Q water, hydrogen peroxide (30% w/v, CAS: 7722-84-1, Fisher Chemical, Pittsburgh, Pensylvania, USA) and ammonia (25%, CAS:7664-42-7, VWR chemicals, Radnor, Pennsylvania, USA) in a volumetric ratio of 5:1:1 for 20 minutes at 80°C, subsequently the substrate is rinsed with Milli-Q water.

Immediately after cleaning, the substrates were either used for experiments, as hydrophilic surfaces, or were further functionalized. The substrate's surface chemistry was tuned through gas phase silanisation. The substrate is placed in a desiccator onto a glass petridish, which is modified in a way, so the glass disk is elevated compared to the functionalization agent. For functionalization two different silanes were used, 1H-1H-2H-2H perfluorodecyltrichlorosilane (97%, stabilized with copper, ABCR, Karlsruhe, Germany) and 3-aminopropyldimethylethoxysilane (97% ABCR, Karlsruhe, Germany). 0.5 mL of silane were placed in a petridish, under argon counter flow, and the desiccator was sealed subsequently by applying vacuum

https://doi.org/10.5194/egusphere-2023-1025
Preprint. Discussion started: 28 June 2023

(Agilent IDP 3, Santa Clara, California, USA). The desiccator was placed in an oven at 40°C for the 1H-1H-2H-2H perfluorodecyltrichlorosilane overnight. After pressurizing, the samples were rinsed with Ethanol (≥99.9%, CAS: 64-17-5, Merck, Darmstadt, Germany) followed by Milli-Q water and immediately used for their respective experiments.

A hydrophilic substrate was prepared as described in Ibrahim et al. (2003), hereafter referred to as substrate b (Θ_S = 55°). Substrates were cleaned with a solution of Nitricacid 65 % (w/w) diluted with distilled water to 50 % (w/w). The substrates were submerged in the Nitricacid for 60s and washed with distilled water for 120 s. Then they were dried in a non-circulating oven at 200 °C for 1h.

A3 Turbulence characteristics

Boundary layer velocities were measured with a CTA at nine heights, ranging from z = 13 mm to z = 245 mm and 13 free stream velocities, ranging from 1.02 m/s to 10.87 m/s. The vertical velocity profiles showed a typical boundary-layer velocity profile for a channel flow. The friction velocity and roughness length were calculated for z $\leq$ 21 mm, where the velocity profile agrees well with the logarithmic law of the wall. The roughness length (z_0) was calculated by extrapolating the logarithmic wind profile to the height z where $\bar{U}$ = 0, giving z_0 = 0.5 mm. The friction velocity (u_*) was computed against the free-stream velocity (U_∞) in two fashions. First, it was derived from the logarithmic wind profile measured in the wind tunnel, assuming the functional form of:

$$u_{*,flux} = \kappa \frac{\delta \overline{U}}{\delta ln(z)}$$

Secondly, u_* was calculated as the arithmetic mean of the directly measured density-normalized momentum flux u_* using the eddy-covariance approach in the vertical profiles:

$$u_{*,EC} = \frac{1}{n} \sum_{i=1}^{n} \sqrt{-\overline{u'w'}_i}$$

Agreement among the two approaches verifies that a turbulent boundary layer has formed (see A3).

The velocities were regressed by a least-squares linear algorithm of the following form:

$$u_* = 0.06 \cdot U_\infty$$

where the uncertainty in u_* is 0.02 ms^{-1} for the 99.7 % percentile.

A4 Impact of relative humidity on detachment for PE42 and PE115

The median detachment $u_{*,th}$ as function of relative humidity (rH) for PE42 and PE115 on hydrophilic to hydrophobic substrates (see Fig.A4).At the observed range of Θ_S, PE42 detaches at higher $u_{*,th}$ and $u_{*,th}$ decreases with Θ_S for both CIMs and CDMs. The bigger PE115 detach at lower $u_{*,th}$ and $u_{*,th}$ varies little with Θ_S. Both PE42 and PE114 show a high $u_{*,th}$ on substrate c. Differences between CIMs and CDMs are small, except for PE115 on substrate c. For substrate a to c, detachment

https://doi.org/10.5194/egusphere-2023-1025
Preprint. Discussion started: 28 June 2023

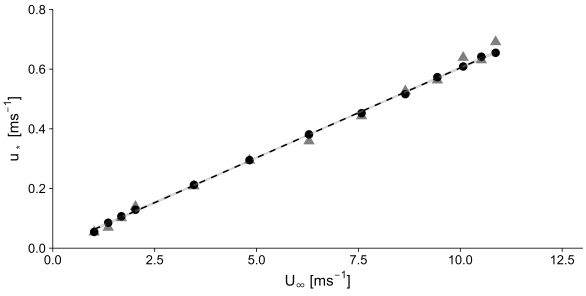

Figure A3. Comparison of the relationship of the free stream velocity U_∞ and friction velocity u_*, by two approaches of determination. The friction velocity was extracted from the logarithmic velocity profile (triangles) and from covariance measurements (dots). The dashed line shows the linear regression of both approaches. $u_* = 0.06 \cdot U_\infty$ R^2 = 0.99

was measured at similar relative humidities. On substrate d, the relative humidities are highest, being close to 50% with at same time overall smallest $u_{*,th}$.

In the observed range of rH, $u_{*,th}$ does not increase with rH. Thus, no indication for the occurrence of capillary forces increasing $u_{*,th}$ is present. Substrate c shows high $u_{*,th}$ at similar rH found for substrate a and b. We would expect that, at a similar rH, $u_{*,th}$ would be lower for substrate c due to the higher hydrophobicity. Substrate d shows smallest median detachment for both PE42 and PE115, fitting the expectation of finding the smallest $u_{*,th}$ for the most hydrophobic substrate.

A5 Scanning electron microscopy

High-resolution images of a polyethylene microsphere (see Fig. A5) and of a borosilicate microsphere (see Fig. A6) were achieved using scanning electron microscopy (Hitachi TM3030, Berkshire, UK).

A6 Microsphere surface roughness

A Dimension Icon AFM (Bruker Corporation Billerica, Massachusetts, USA) equipped with a NanoScope V controller was used to determine the surface roughness of PE69 and GL69. For imaging, OMCL-AC160TS cantilevers (Olympus, nominal spring constant 26 N/m, nominal resonance frequency 300 kHz) were used. The tapping mode frequency was set to 95% of the cantilevers actual resonance frequency with an excitation amplitude of 500 mV and an amplitude setpoint of 400 mV. The AFM images were processed with NanoScope Analysis software (version 1.80, Bruker Nano Inc.). The root-mean-square roughness for PE69 and GL69 was 248.5 $\pm$ 32.2 nm and 27.7 $\pm$ 9.0 nm, respectively (see Fig. A7 and Fig. A8).

A7 How collisions independent microsphere were determined

The following pseudocode outlines the process of defining windward microspheres. First, all microspheres within the field of observation are identified and added to a list of windward microspheres. For each microsphere in the list, two vectors are drawn from its center that have the same direction as the airflow. These vectors are then rotated 15° around the center of the

https://doi.org/10.5194/egusphere-2023-1025
Preprint. Discussion started: 28 June 2023

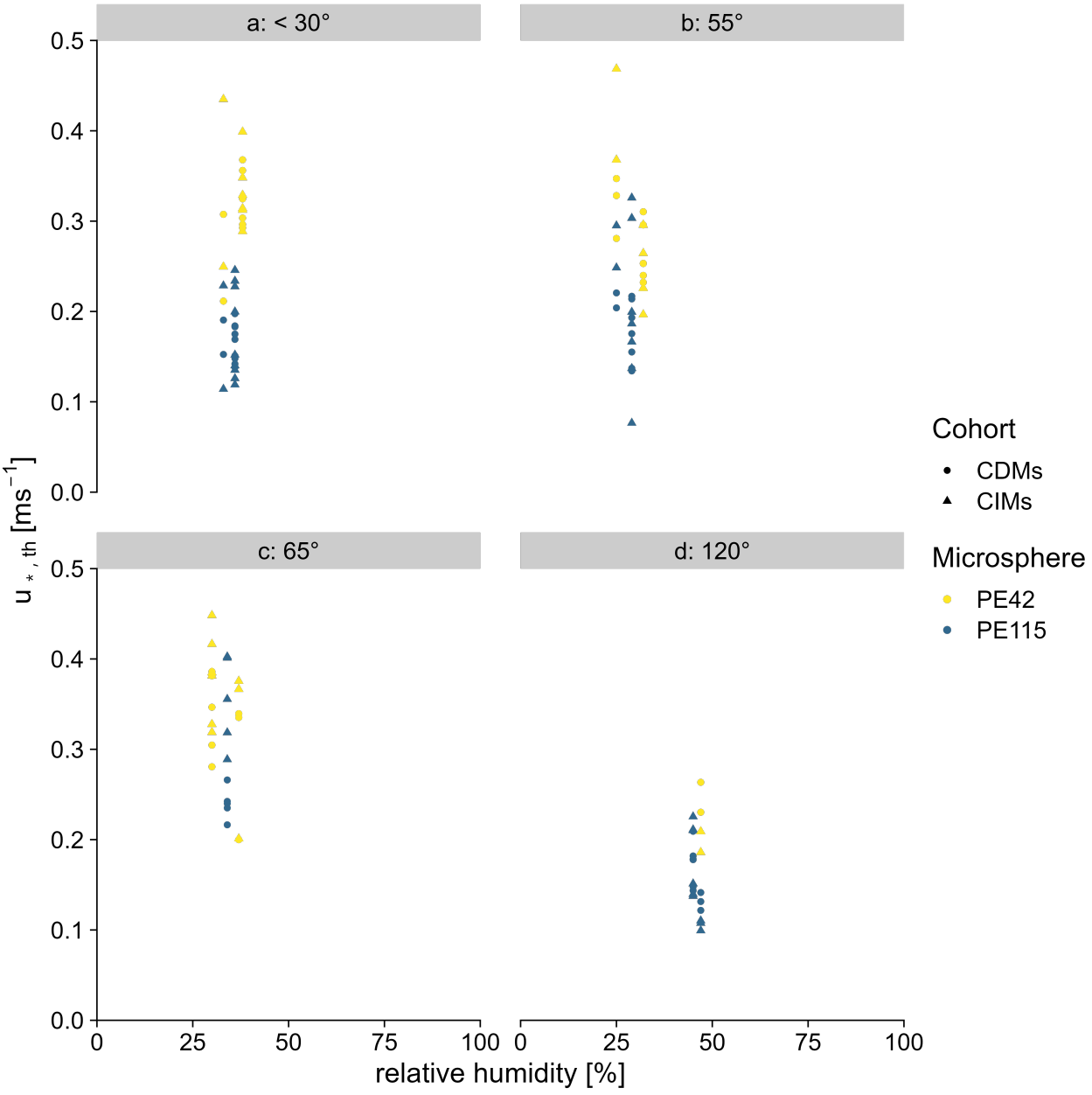

Figure A4. Median detachment $u_{*,th}$ as function of relative humidity for polyethylene microspheres with diameters: 38-45 μm (PE42) and 105-126 μm (PE115) on hydrophilic to hydrophobic substrates. The hydrophobicity is defined as the static contact angle between the substrate and a water droplet (Θ_S) using the sessile drop method. Hydrophobicity increases from small to high angles. Indices a to d indicate the individual substrates according to Tab. 1.

https://doi.org/10.5194/egusphere-2023-1025
Preprint. Discussion started: 28 June 2023

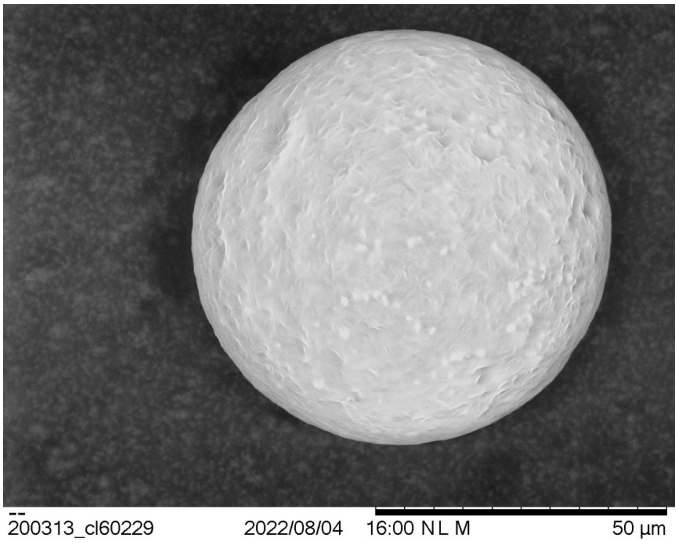

Figure A5. Scanning electron microscope image of a polyethylene microsphere.

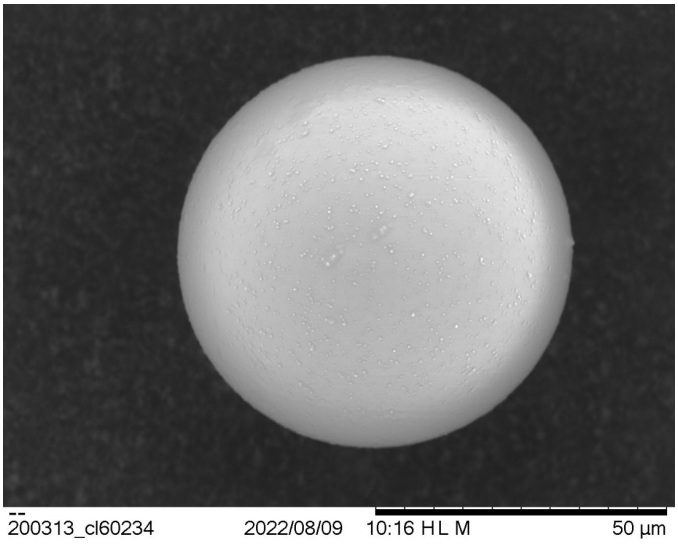

Figure A6. Scanning electron microscope image of a borosilicate microsphere.

https://doi.org/10.5194/egusphere-2023-1025
Preprint. Discussion started: 28 June 2023

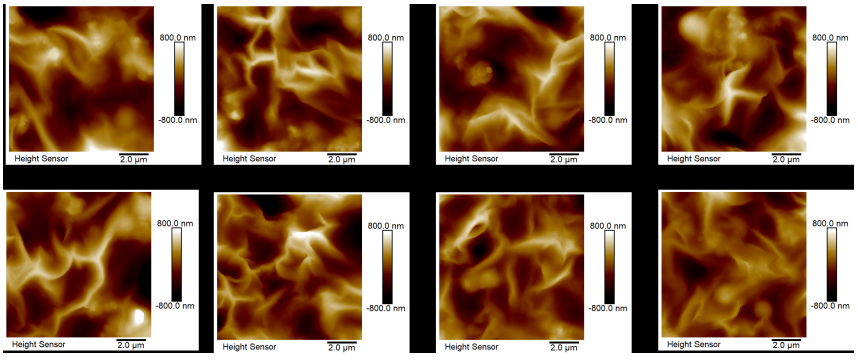

Figure A7. Atomic force microscopy image of a polyethylene microsphere.

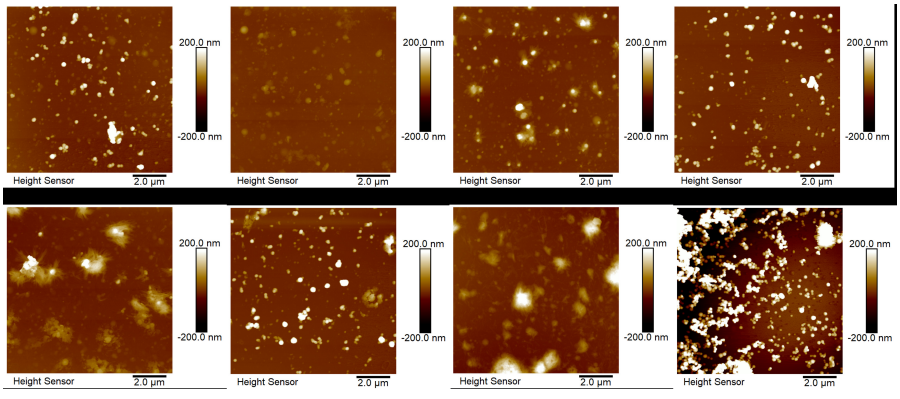

Figure A8. Atomic force microscopy image of a borosilicate microsphere.

respective microspheres, with one vector rotating clockwise and the other rotating counterclockwise. As a result, the vectors form a 30° angle, and the area within this triangle is assumed to be the space that the microsphere would pass through after detaching. Consequently, any microspheres within this area are removed from the list of windward microspheres, since they are assumed to be affected by collisions with other microspheres. Once the list has been iterated through completely, it only contains windward microspheres.

Author contributions. EME planned and conducted the wind tunnel experiments and wrote the manuscript; SS and IK provided and characterized the substrates and characterized the microspheres; GP, WB and CKT supervised the writing and experimental process

Competing interests. The authors declare that they have no competing interests.

https://doi.org/10.5194/egusphere-2023-1025
Preprint. Discussion started: 28 June 2023

Acknowledgements. Funded by the Deutsche Forschungsgemeinschaft (DFG, German Research Foundation) – Project Number 391977956 – SFB 1357 and 491183248. Funded by the Open Access Publication Fund of the University of Bayreuth.

https://doi.org/10.5194/egusphere-2023-1025
Preprint. Discussion started: 28 June 2023

References

Alexiadou, P., Foskolos, I., and Frantzis, A.: Ingestion of macroplastics by odontocetes of the Greek Seas, Eastern Mediterranean: Often deadly!, Marine Pollution Bulletin, 146, 67–75, https://doi.org/10.1016/j.marpolbul.2019.05.055, 2019.

Allen, S., Allen, D., Phoenix, V. R., Roux, G. L., Jiménez, P. D., Simonneau, A., Binet, S., and Galop, D.: Atmospheric transport and deposition of microplastics in a remote mountain catchment, Nature Geoscience, 12, 339–344, https://doi.org/10.1038/s41561-019-0335-5, number: 5 Publisher: Nature Publishing Group, 2019.

Allen, S., Allen, D., Baladima, F., Phoenix, V. R., Thomas, J. L., Le Roux, G., and Sonke, J. E.: Evidence of free tropospheric and long-range transport of microplastic at Pic du Midi Observatory, Nature Communications, 12, 7242, https://doi.org/10.1038/s41467-021-27454-7, number: 1 Publisher: Nature Publishing Group, 2021.

Allen, S., Allen, D., Karbalaei, S., Maselli, V., and Walker, T. R.: Micro(nano)plastics sources, fate, and effects: What we know after ten years of research, Journal of Hazardous Materials Advances, 6, 100 057, https://doi.org/10.1016/j.hazadv.2022.100057, 2022.

Bank, M. S. and Hansson, S. V.: The Plastic Cycle: A Novel and Holistic Paradigm for the Anthropocene, Environmental Science & Technology, 53, 7177–7179, https://doi.org/10.1021/acs.est.9b02942, publisher: American Chemical Society, 2019.

Barnes, D. K. A., Galgani, F., Thompson, R. C., and Barlaz, M.: Accumulation and fragmentation of plastic debris in global environments, Philosophical Transactions of the Royal Society B: Biological Sciences, 364, 1985–1998, https://doi.org/10.1098/rstb.2008.0205, publisher: Royal Society, 2009.

Bergmann, M., Mützel, S., Primpke, S., Tekman, M. B., Trachsel, J., and Gerdts, G.: White and wonderful? Microplastics prevail in snow from the Alps to the Arctic, Science Advances, 5, eaax1157, https://doi.org/10.1126/sciadv.aax1157, number: 8 Publisher: American Association for the Advancement of Science Section: Research Article, 2019.

Boos, J.-P., Gilfedder, B. S., and Frei, S.: Tracking Microplastics Across the Streambed Interface: Using Laser-Induced-Fluorescence to Quantitatively Analyze Microplastic Transport in an Experimental Flume, Water Resources Research, 57, e2021WR031 064, https://doi.org/10.1029/2021WR031064, _eprint: https://onlinelibrary.wiley.com/doi/pdf/10.1029/2021WR031064, 2021.

Brahney, J., Hallerud, M., Heim, E., Hahnenberger, M., and Sukumaran, S.: Plastic rain in protected areas of the United States, Science, 368, 1257–1260, https://doi.org/10.1126/science.aaz5819, number: 6496, 2020.

Bullard, J. E., Ockelford, A., O'Brien, P., and McKenna Neuman, C.: Preferential transport of microplastics by wind, Atmospheric Environment, 245, 118 038, https://doi.org/10.1016/j.atmosenv.2020.118038, 2021.

Carlin, J., Craig, C., Little, S., Donnelly, M., Fox, D., Zhai, L., and Walters, L.: Microplastic accumulation in the gastrointestinal tracts in birds of prey in central Florida, USA, Environmental Pollution, 264, 114 633, https://doi.org/10.1016/j.envpol.2020.114633, 2020.

Chia, R. W., Lee, J.-Y., Kim, H., and Jang, J.: Microplastic pollution in soil and groundwater: a review, Environmental Chemistry Letters, 19, 4211–4224, https://doi.org/10.1007/s10311-021-01297-6, 2021.

Corn, M. and Stein, F.: Re-entrainment of Particles from a Plane Surface, American Industrial Hygiene Association Journal, 26, 325–336, https://doi.org/10.1080/00028896509342739, 1965.

de Souza Machado, A. A., Lau, C. W., Till, J., Kloas, W., Lehmann, A., Becker, R., and Rillig, M. C.: Impacts of Microplastics on the Soil Biophysical Environment, Environmental Science & Technology, 52, 9656–9665, https://doi.org/10.1021/acs.est.8b02212, publisher: American Chemical Society, 2018.

Donnelly-Greenan, E. L., Nevins, H. M., and Harvey, J. T.: Entangled seabird and marine mammal reports from citizen science surveys from coastal California (1997–2017), Marine Pollution Bulletin, 149, 110 557, https://doi.org/10.1016/j.marpolbul.2019.110557, 2019.

https://doi.org/10.5194/egusphere-2023-1025
Preprint. Discussion started: 28 June 2023

Dris, R., Gasperi, J., Rocher, V., Saad, M., Renault, N., Tassin, B., Dris, R., Gasperi, J., Rocher, V., Saad, M., Renault, N., and Tassin, B.: Microplastic contamination in an urban area: a case study in Greater Paris, Environmental Chemistry, 12, 592–599, https://doi.org/10.1071/EN14167, publisher: CSIRO PUBLISHING, 2015.

Du, H., Xie, Y., and Wang, J.: Microplastic degradation methods and corresponding degradation mechanism: Research status and future perspectives, Journal of Hazardous Materials, 418, 126 377, https://doi.org/10.1016/j.jhazmat.2021.126377, 2021.

Esders, E. M., Georgi, C., Babel, W., and Thomas, C. K.: Quantitative detection of aerial suspension of particles with a full-frame visual camera for atmospheric wind tunnel studies, Aerosol Science and Technology, 56, 530–544, https://doi.org/10.1080/02786826.2022.2048789, 2022.

Evangeliou, N., Grythe, H., Klimont, Z., Heyes, C., Eckhardt, S., Lopez-Aparicio, S., and Stohl, A.: Atmospheric transport is a major pathway of microplastics to remote regions, Nature Communications, 11, 3381, https://doi.org/10.1038/s41467-020-17201-9, 2020.

Geyer, R., Jambeck, J. R., and Law, K. L.: Production, use, and fate of all plastics ever made, Science Advances, 3, e1700 782, https://doi.org/10.1126/sciadv.1700782, publisher: American Association for the Advancement of Science, 2017.

Horton, A. A. and Dixon, S. J.: Microplastics: An introduction to environmental transport processes, WIREs Water, 5, e1268, https://doi.org/10.1002/wat2.1268, _eprint: https://onlinelibrary.wiley.com/doi/pdf/10.1002/wat2.1268, 2018.

Ibrahim, A., Dunn, P., and Brach, R.: Microparticle detachment from surfaces exposed to turbulent air flow: Effects of flow and particle deposition characteristics, Journal of Aerosol Science, 35, 805–821, https://doi.org/10.1016/j.jaerosci.2004.01.002, 2004.

Ibrahim, A. H., Dunn, P. F., and Brach, R. M.: Microparticle detachment from surfaces exposed to turbulent air flow: controlled experiments and modeling, Journal of Aerosol Science, 34, 765–782, https://doi.org/10.1016/S0021-8502(03)00031-4, 2003.

Kassab, A. S., Ugaz, V. M., King, M. D., and Hassan, Y. A.: High Resolution Study of Micrometer Particle Detachment on Different Surfaces, Aerosol Science and Technology, 47, 351–360, https://doi.org/10.1080/02786826.2012.752789, publisher: Taylor & Francis _eprint: https://doi.org/10.1080/02786826.2012.752789, 2013.

Katija, K., Choy, C. A., Sherlock, R. E., Sherman, A. D., and Robison, B. H.: From the surface to the seafloor: How giant larvaceans transport microplastics into the deep sea, Science Advances, 3, e1700 715, https://doi.org/10.1126/sciadv.1700715, publisher: American Association for the Advancement of Science Section: Research Article, 2017.

Kern, W.: The Evolution of Silicon Wafer Cleaning Technology, Journal of The Electrochemical Society, 137, 1887, https://doi.org/10.1149/1.2086825, 1990.

Kernchen, S., Löder, M. G. J., Fischer, F., Fischer, D., Moses, S. R., Georgi, C., Nölscher, A. C., Held, A., and Laforsch, C.: Airborne microplastic concentrations and deposition across the Weser River catchment, Science of The Total Environment, 818, 151 812, https://doi.org/10.1016/j.scitotenv.2021.151812, 2022.

Kim, Y., Wellum, G., Mello, K., Strawhecker, K. E., Thoms, R., Giaya, A., and Wyslouzil, B. E.: Effects of relative humidity and particle and surface properties on particle resuspension rates, Aerosol Science and Technology, 50, 339–352, https://doi.org/10.1080/02786826.2016.1152350, number: 4, 2016.

Klein, M. and Fischer, E. K.: Microplastic abundance in atmospheric deposition within the Metropolitan area of Hamburg, Germany, Science of The Total Environment, 685, 96–103, https://doi.org/10.1016/j.scitotenv.2019.05.405, 2019.

Lehmann, A., Leifheit, E. F., Gerdawischke, M., and Rillig, M. C.: Microplastics have shape- and polymer-dependent effects on soil aggregation and organic matter loss – an experimental and meta-analytical approach, Microplastics and Nanoplastics, 1, 7, https://doi.org/10.1186/s43591-021-00007-x, 2021.

https://doi.org/10.5194/egusphere-2023-1025
Preprint. Discussion started: 28 June 2023

Li, P., Wang, X., Su, M., Zou, X., Duan, L., and Zhang, H.: Characteristics of Plastic Pollution in the Environment: A Review, Bulletin of Environmental Contamination and Toxicology, https://doi.org/10.1007/s00128-020-02820-1, 2020.

Mckenna Neuman, C.: Effects of Temperature and Humidity upon the Entrainment of Sedimentary Particles by Wind, Boundary-Layer Meteorology, 108, 61–89, https://doi.org/10.1023/A:1023035201953, 2003.

Meides, N., Menzel, T., Poetzschner, B., Löder, M. G. J., Mansfeld, U., Strohriegl, P., Altstaedt, V., and Senker, J.: Reconstructing the Environmental Degradation of Polystyrene by Accelerated Weathering, Environmental Science & Technology, https://doi.org/10.1021/acs.est.0c07718, publisher: American Chemical Society, 2021.

Nizzetto, L., Futter, M., and Langaas, S.: Are Agricultural Soils Dumps for Microplastics of Urban Origin?, Environmental Science & Technology, 50, 10 777–10 779, https://doi.org/10.1021/acs.est.6b04140, publisher: American Chemical Society, 2016.

Rabinovich, Y. I., Adler, J. J., Esayanur, M. S., Ata, A., Singh, R. K., and Moudgil, B. M.: Capillary forces between surfaces with nanoscale roughness, Advances in Colloid and Interface Science, 96, 213–230, https://doi.org/10.1016/S0001-8686(01)00082-3, 2002.

Ravi, S., D'Odorico, P., Over, T. M., and Zobeck, T. M.: On the effect of air humidity on soil susceptibility to wind erosion: The case of air-dry soils, Geophysical Research Letters, 31, https://doi.org/10.1029/2004GL019485, _eprint: https://onlinelibrary.wiley.com/doi/pdf/10.1029/2004GL019485, 2004.

Rehm, R., Zeyer, T., Schmidt, A., and Fiener, P.: Soil erosion as transport pathway of microplastic from agriculture soils to aquatic ecosystems, Science of The Total Environment, 795, 148 774, https://doi.org/10.1016/j.scitotenv.2021.148774, 2021.

Rezaei, M., Riksen, M. J., Sirjani, E., Sameni, A., and Geissen, V.: Wind erosion as a driver for transport of light density microplastics, Science of The Total Environment, 669, 273–281, https://doi.org/10.1016/j.scitotenv.2019.02.382, 2019.

Rillig, M. C.: Microplastic in Terrestrial Ecosystems and the Soil?, Environmental Science & Technology, 46, 6453–6454, https://doi.org/10.1021/es302011r, publisher: American Chemical Society, 2012.

Rolf, M., Laermanns, H., Kienzler, L., Pohl, C., Möller, J. N., Laforsch, C., Löder, M. G. J., and Bogner, C.: Flooding frequency and floodplain topography determine abundance of microplastics in an alluvial Rhine soil, Science of The Total Environment, 836, 155 141, https://doi.org/10.1016/j.scitotenv.2022.155141, 2022.

Shao, Y. and Lu, H.: A simple expression for wind erosion threshold friction velocity, Journal of Geophysical Research: Atmospheres, 105, 22 437–22 443, https://doi.org/10.1029/2000JD900304, 2000.

Shiu, R.-F., Chen, L.-Y., Lee, H.-J., Gong, G.-C., and Lee, C.: New insights into the role of marine plastic-gels in microplastic transfer from water to the atmosphere via bubble bursting, Water Research, 222, 118 856, https://doi.org/10.1016/j.watres.2022.118856, 2022.

Shruti, V. C., Kutralam-Muniasamy, G., Pérez-Guevara, F., Roy, P. D., and Martínez, I. E.: Occurrence and characteristics of atmospheric microplastics in Mexico City, Science of The Total Environment, p. 157601, https://doi.org/10.1016/j.scitotenv.2022.157601, 2022.

Soltani, M. and Ahmadi, G.: On particle adhesion and removal mechanisms in turbulent flows, Journal of Adhesion Science and Technology, 8, 763–785, https://doi.org/10.1163/156856194X00799, publisher: Taylor & Francis _eprint: https://doi.org/10.1163/156856194X00799, 1994.

Stefánsson, H., Peternell, M., Konrad-Schmolke, M., Hannesdóttir, H., Ásbjörnsson, E. J., and Sturkell, E.: Microplastics in Glaciers: First Results from the Vatnajökull Ice Cap, Sustainability, 13, 4183, https://doi.org/10.3390/su13084183, number: 8 Publisher: Multidisciplinary Digital Publishing Institute, 2021.

Thrift, E., Porter, A., Galloway, T. S., Coomber, F. G., and Mathews, F.: Ingestion of plastics by terrestrial small mammals, Science of The Total Environment, 842, 156 679, https://doi.org/10.1016/j.scitotenv.2022.156679, 2022.

https://doi.org/10.5194/egusphere-2023-1025
Preprint. Discussion started: 28 June 2023

Thushari, G. G. N. and Senevirathna, J. D. M.: Plastic pollution in the marine environment, Heliyon, 6, e04 709, https://doi.org/10.1016/j.heliyon.2020.e04709, 2020.

Tian, X., Yang, M., Guo, Z., Chang, C., Li, J., Guo, Z., Wang, R., Li, Q., and Zou, X.: Plastic mulch film induced soil microplastic enrichment and its impact on wind-blown sand and dust, Science of The Total Environment, 813, 152 490, https://doi.org/10.1016/j.scitotenv.2021.152490, 2022.

Ugwu, K., Herrera, A., and Gómez, M.: Microplastics in marine biota: A review, Marine Pollution Bulletin, 169, 112 540, https://doi.org/10.1016/j.marpolbul.2021.112540, 2021.

Wang, F., Wang, Q., Adams, C. A., Sun, Y., and Zhang, S.: Effects of microplastics on soil properties: Current knowledge and future perspectives, Journal of Hazardous Materials, 424, 127 531, https://doi.org/10.1016/j.jhazmat.2021.127531, 2022.

Weinstein, J. E., Crocker, B. K., and Gray, A. D.: From macroplastic to microplastic: Degradation of high-density polyethylene, polypropylene, and polystyrene in a salt marsh habitat, Environmental Toxicology and Chemistry, 35, 1632–1640, https://doi.org/10.1002/etc.3432, _eprint: https://onlinelibrary.wiley.com/doi/pdf/10.1002/etc.3432, 2016.

Windsor, F. M., Durance, I., Horton, A. A., Thompson, R. C., Tyler, C. R., and Ormerod, S. J.: A catchment-scale perspective of plastic pollution, Global Change Biology, 25, 1207–1221, https://doi.org/10.1111/gcb.14572, _eprint: https://onlinelibrary.wiley.com/doi/pdf/10.1111/gcb.14572, 2019.

Xu, B., Liu, F., Cryder, Z., Huang, D., Lu, Z., He, Y., Wang, H., Lu, Z., Brookes, P. C., Tang, C., Gan, J., and Xu, J.: Microplastics in the soil environment: Occurrence, risks, interactions and fate – A review, Critical Reviews in Environmental Science and Technology, 50, 2175–2222, https://doi.org/10.1080/10643389.2019.1694822, publisher: Taylor & Francis _eprint: https://doi.org/10.1080/10643389.2019.1694822, 2020.

Yang, M., Tian, X., Guo, Z., Chang, C., Li, J., Guo, Z., Li, H., Liu, R., Wang, R., Li, Q., and Zou, X.: Effect of Dry Soil Aggregate Size on Microplastic Distribution and Its Implications for Microplastic Emissions Induced by Wind Erosion, Environmental Science & Technology Letters, 9, 618–624, https://doi.org/10.1021/acs.estlett.2c00338, 2022.

Zhang, J., Ren, S., Xu, W., Liang, C., Li, J., Zhang, H., Li, Y., Liu, X., Jones, D. L., Chadwick, D. R., Zhang, F., and Wang, K.: Effects of plastic residues and microplastics on soil ecosystems: A global meta-analysis, Journal of Hazardous Materials, 435, 129 065, https://doi.org/10.1016/j.jhazmat.2022.129065, 2022.

Zhang, Y.: Atmospheric microplastics_ A review on current status and perspectives, Earth Science Reviews, p. 15, 2020.